PHYSICAL REVIEW B **94**, 060102(R) (2016)

Evidence for near-infrared photoluminescence of nitrogen vacancy centers in 4*H*-SiC

S. A. Zargaleh,[1,2,*] B. Eble,[2] S. Hameau,[2] J.-L. Cantin,[2] L. Legrand,[2] M. Bernard,[2] F. Margaillan,[2] J.-S. Lauret,[1] J.-F. Roch,[1] H. J. von Bardeleben,[2] E. Rauls,[3] U. Gerstmann,[3,†] and F. Treussart[1,‡]

[1]*Laboratoire Aimé Cotton, CNRS, Univ. Paris-Sud, ENS Cachan, Université Paris-Saclay, 91405 Orsay Cedex, France*

[2]*Sorbonne Universités, UPMC Université Paris 06, CNRS-UMR 7588, Institut des NanoSciences de Paris, 75005 Paris, France*

[3]*Lehrstuhl für Theoretische Physik, Universität Paderborn, 33098 Paderborn, Germany*

(Received 6 June 2016; revised manuscript received 18 July 2016; published 5 August 2016)

We present evidence of near-infrared photoluminescence (PL) signature of nitrogen vacancy centers $(N_CV_{Si})^-$ in silicon carbide (SiC). This center exhibits an $S = 1$ ground state spin similar to the NV^- center in diamond. We have performed photoluminescence excitation measurements at cryogenic temperature and demonstrated efficient photoexcitation of distinct photoluminescence from $(N_CV_{Si})^-$ in 4*H*-SiC. Furthermore, by correlating the energies of measured zero phonon lines (ZPLs) with theoretical values derived from hybrid density functional theory each of the ZPLs has been associated to the respective occupation of hexagonal (*h*) and quasicubic (*k*) lattice sites in close analogy to neutral divacancy centers $(V_CV_{Si})^0$ in the same material. Finally, with the appropriate choice of excitation energy we demonstrated the selective excitation of $(N_CV_{Si})^-$ PL with no contamination by $(V_CV_{Si})^0$ PL, thereby opening the way towards the optical detection of $(N_CV_{Si})^-$ electron spin resonance.

DOI: 10.1103/PhysRevB.94.060102

Paramagnetic point defects deep in wide band-gap semiconductors are of special interest. Well isolated from the environment, these defects possess remarkable long spin coherence time and have proven to be potent nanoscale systems for solid-state quantum information processing and sensing [1]. Among various optically active point defects the negatively charged nitrogen vacancy (NV^-) centre in diamond is a prominent one, exhibiting an optically detectable electron spin $S = 1$ magnetic resonance with unrivaled photostability and high quantum yield at room temperature [2]. These spin properties have allowed diverse applications such as entanglement [3], quantum memory [4], nanoscale nuclear magnetic resonance imaging [5], quantum biosensing [6], and nanoscale electric field [7], magnetic field [8], and temperature sensing [9] (for a review, see Ref. [10]). Recently, efforts have been directed towards the identification and engineering of similar defects in alternative wide-band-gap semiconductors, which are optically active in different spectral domains.

Among these materials, silicon carbide (SiC) has attracted the greatest attention because its growth at controlled *n*- or *p*-doping levels is mastered by semiconductor industry. It exists in a wealth of different crystal structures with three main polytypes: 4*H*, 6*H* (hexagonal) and 3*C* (cubic), that can be grown in a highly reproducible manner. This structural variety offers a broad range of possible point defects adapted to the above mentioned applications [11,12], among which are the carbon antisite-vacancy pair ($C_{Si}V_C$) [13–16], the silicon monovacancy V_{Si}^- [11,17–21], and the neutral divacancy $(V_CV_{Si})^0$ [12,15,22–24]. Similar to NV^- in diamond, the electronic ground state of $(V_CV_{Si})^0$ in 4*H*-SiC is a spin triplet ($S = 1$) in which magnetic resonance can be optically detected in near-infrared light of 1.09–1.16 eV (1069–1137 nm), with an associated zero-field splitting of $D \approx 1.3$ GHz [23]. Theoretical work has proposed the nitrogen vacancy $(N_CV_{Si})^-$ center in SiC [25,26] as another optically active defect with an electronic structure strongly resembling that of the divacancies in silicon carbide [27] and that of NV^- center in diamond.

In the present investigation, we focus on the 4*H*-SiC polytype in which there are two nonequivalent lattice sites. Therefore, the simplest defect forms two different structures giving rise to different photoluminescence signatures (two ZPLs) known as V_1 and V_2 in the case of the V_{Si}^- center [28]. For the $(V_CV_{Si})^0$ divacancy and for the $(N_CV_{Si})^-$ center, the two adjacent defects of the pair not only differ in lattice sites but also in orientation, organizing either in axial (*hh*,*kk*) or in basal (*hk*, *kh*) configuration [22] as displayed in Fig. 1. Each configuration has its own site specific zero phonon line (ZPL), which has been labeled PL1–PL4 in previous studies of $(V_CV_{Si})^0$ [23].

Recently, the $(N_CV_{Si})^-$ defect has been detected by electron paramagnetic resonance (EPR) in high energy proton irradiated and high temperature annealed bulk 4*H*-SiC. $(N_CV_{Si})^-$ EPR signal was observed under thermal equilibrium as well as under photoexcitation (photo-EPR) [27]. Like the divacancy, the $(N_CV_{Si})^-$ ground state is a ^3A triplet ($S = 1$) that can be optically polarized with high efficiency. Moreover, the spin Hamiltonian parameters were measured to be very close to those of the divacancy. Here we report on the observation of distinct ZPLs that we associate to $(N_CV_{Si})^-$ by comparison of their energies to *ab initio* calculations based on hybrid DFT. These ZPLs are located in the 0.99–1.06 eV energy range corresponding to 1170–1250 nm wavelength. This near-infrared spectral region is well adapted to coupling to a high quality factor photonic crystal microcavity [29] with lower Rayleigh scattering losses than emitters in the visible range.

To investigate the photoluminescence (PL) signature of $(N_CV_{Si})^-$ centers in SiC, we used the same sample as the one investigated by photo-EPR in Ref. [27]. Briefly, this sample is a 300-μm-thick *n*-type 4*H*-SiC slab (nitrogen doped at concentration 2×10^{17} cm^{-3}) irradiated with high energy protons at 10^{16} cm^{-2} fluence. At 12 MeV, the protons cross the sample to full extent and introduce defects in both the

*soroush.abbasizargaleh@ens-cachan.fr
†uwe.gerstmann@upb.de
‡francois.treussart@ens-cachan.fr

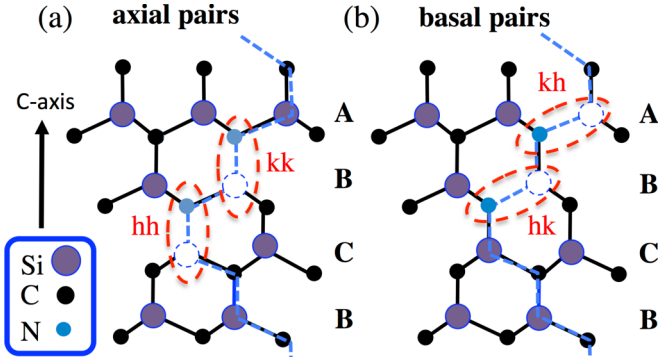

FIG. 1. Orientation of defect pairs (here N_CV_{Si}) in 4H-SiC. The pairs are surrounded by dashed ovals. (a) kk/hh axial pairs. (b) kh/hk basal pairs. Empty sites are represented by dashed circles. In the case of divacancies V_CV_{Si}, the neighboring N_C sites in the ovals become also empty.

carbon and silicon sublattices, mainly monovacancies and carbon split interstitials $(CC)_C$ [27]. To generate $(N_CV_{Si})^-$ centers the sample has been subsequently annealed at 900 °C under vacuum, showing the characteristic nitrogen-related EPR spectra afterwards . We first investigated the PL intensity at room temperature at different sample locations, by raster scanning a laser beam focused onto the sample. We used three different excitation laser wavelengths (405, 532, and 633 nm), and a near-infrared-optimized imaging spectrograph equipped with a liquid-nitrogen cooled InGaAs photodiode array. In all cases we observed a broad emission spectra, but centered on 1.23 eV (1012 nm) for 633 nm excitation, and 0.97 eV (1281 nm) for 405 and 532 nm excitations (see Supplemental Material [30]). The PL intensity from the sample was uniform, which is in agreement with the homogeneous proton irradiation.

We then studied the PL at cryogenic temperatures. The sample was mounted on the cold finger of a helium-flow cryostat with optical access and cooled down to about 10 K. We used a tunable titanium-sapphire laser in a pseudocontinuous wave mode. The laser was focused onto the sample with a microscope objective (magnification ×32, numerical aperture 0.6), and the PL collected through the same objective was filtered from the remaining pump light by a long-pass filter (cut-off at 1.165 eV) before being sent to the imaging spectrograph. Figure 2(a) shows the photoluminescence excitation (PLE) spectral map obtained when we varied the excitation energy in the 1.734–1.240 eV (715–1000 nm) range. Figure 2(b) displays the PL spectra at 1.653 and 1.240 eV excitation wavelengths. The ZPLs of the divacancies $(V_CV_{Si})^0$ labeled PL1–PL4 and already identified in previous work [23] can be detected at $E_{exc} = 1.653$ eV excitation energy and almost totally disappear at $E_{exc} = 1.240$ eV. For $E_{exc} \lesssim 1.653$ eV, distinct ZPLs labeled PLX1–PLX6 appear in the 0.99–1.06 eV energy range (spectral range 1170–1250 nm) which were not reported in previous studies. At lower energy, one can identify the α/β lines of substitutional vanadium ions (V_{Si}^{4+}) [31]. We did not observe the Si vacancy V1/V2 lines, which are expected in the 1.459–1.348 eV energy range. This confirms the general finding that Si vacancies are annealed out for temperatures above 750 °C [32].

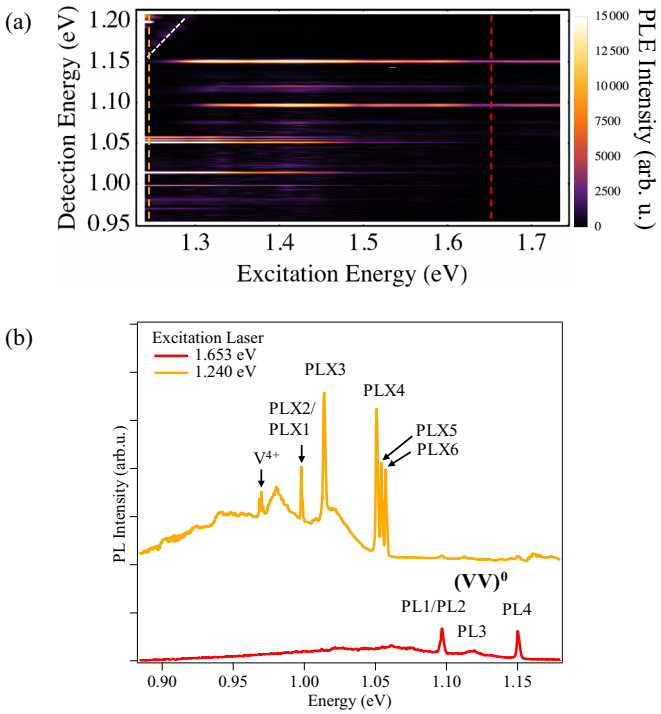

FIG. 2. Cryogenic temperature (10 K) PLE of a proton irradiated, high temperature annealed 4H-SiC sample. (a) PLE intensity map taken with 17 meV-increment excitation; broadband background (from phonon sidebands) was subtracted. The inclined dashed line is superimposed on the Raman LO line. (b) PL spectra at 1.653 eV and 1.240 eV excitation energies, indicated by vertical dashed lines in (a). In addition to the divacancy ZPLs (PL1–PL4), new ZPLs (PLX1–PLX6) are observed (vanadium-related ZPLs marked with V^{4+}).

In order to associate some of these ZPLs (PLX1–PLX6) to the previously observed EPR-active $(N_CV_{Si})^-$ defects [27], we relied on three complementary pieces of information: (i) the comparison of the relative positions of the PLX1–PLX6 lines to those of $(V_CV_{Si})^0$ PL1–PL4 ZPLs; (ii) the variation of intensity of each ZPL with the excitation wavelength; and (iii) a DFT total energy calculation of NV center ZPL energies for the four crystallographic configurations. We have analyzed and plotted in Fig. 3 PLX1–PLX6 and vanadium V^{4+} line intensities for excitation energies varying in the 1.734–1.240 eV range. We observe over the whole spectral range explored that the intensities of PLX5 and PLX6 superimpose well like those of the vanadium (V^{4+}) α/β lines. From the literature we found that PLX5–PLX6 are within ≈3 meV in energy to the two ZPLs of the UD-1 defect (reported at 1.0596 and 1.0586 eV in 4H-SiC [33]). Since UD-1 appeared after doping with tungsten, it was related to this impurity in substitutional position (W_{Si}). Although our sample was not intentionally doped with tungsten, this element could come from crucibles or furnace components and may have diffused inside the sample during the annealing process. Therefore, we are left with the four, still unidentified, PLX1–PLX4 lines.

In Ref. [27] it has been established by photo-EPR measurements and comparative DFT calculations that the electronic structure of the $(N_CV_{Si})^-$ centers closely resembles that of

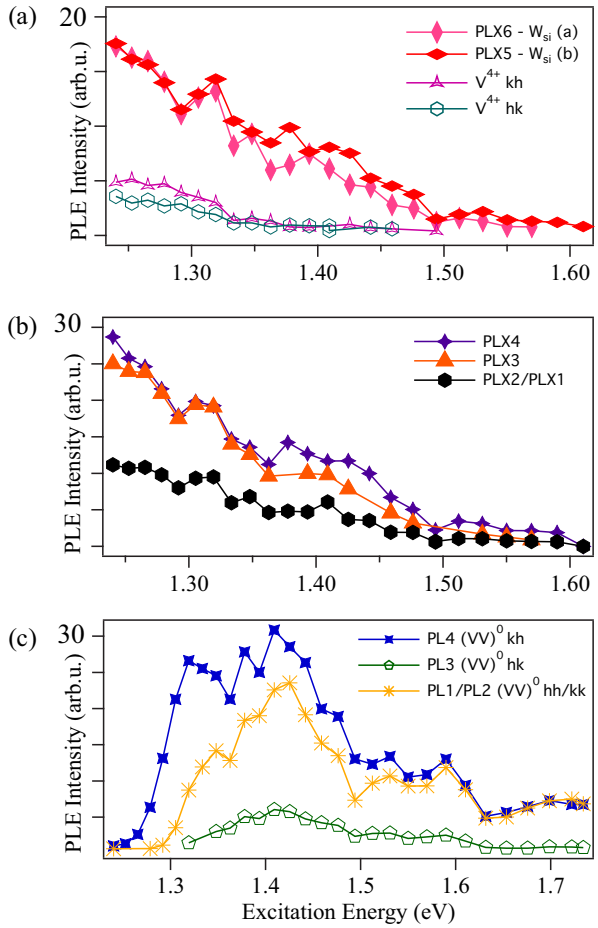

FIG. 3. Intensities of individual ZPLs observed in Fig. 2 by PLE (10 K) as given by the amplitudes of the Gaussian functions used to fit each ZPL. Intensities of (a) vanadium defect-related ZPLs and PLX5/6 ZPL (potentially related to tungsten impurities), (b) distinct ZPLs which we attribute to NV centers in 4H-SiC, and (c) divacancy axial and basal pairs.

the $(V_C V_{Si})^0$ centers in 4H-SiC. Hence, in analogy to the divacancies, *four* NV-related ZPLs for the *four* different pair orientations are expected, providing a possible explanation for the remaining PLX1–PLX4 lines. Note that this scenario is also in line with the reappearance of both photo-EPR and PL signals at excitation energy larger than 2.3 eV (see Ref. [27] and the Supplemental Material [30]). Indeed, following Ref. [27], we propose that this effect is due to indirect, e.g., hole-assisted, excitation requiring higher energy excitation, which explains why PL and photo-EPR signals are weak in the intermediate 1.6–2.1 eV excitation energy range. The attribution of the PLX1–PLX4 lines to the $(N_C V_{Si})^-$ center is further supported by DFT total energy calculations for the ZPL transition energies which we have performed with the QUANTUM ESPRESSO package [34] following exactly the same approach as in Ref. [27]. To model divacancy and nitrogen vacancy centers in 4H-SiC, we used supercells of hexagonal shape containing up to 432 atoms, standard norm conserving pseudopotentials, and a plane-wave basis with 50 Ry energy cutoff. First, all defect structures have been fully relaxed for the $^3A_2$-like ground states as well as for the ^3E-like excited states using shifted $2 \times 2 \times 2$ Monkhorst-Pack k-point samplings and the spin-polarized Perdew-Burke-Ernzerhof (PBE) functional [35]. In order to obtain accurate transition energies for the defect states relaxed this way, we performed total energy calculations with the gap-correcting Heyd-Scuseria-Ernzerhof (HSE) hybrid functional [36].

The calculated adiabatic transition energies for the $(^3E \rightarrow {}^3A_2)$-like internal transitions and different defect pair orientations are compiled in Table I. For both the divacancy and the $(N_C V_{Si})^-$ defects, and for each orientation, we obtain good agreement between calculated and measured energies. The calculation yield slightly underestimated splittings between the ZPL originating from the two basal pairs hk and kh. Furthermore, the quasidegeneracies of the "axial" ZPL lines are less pronounced in the calculation. We attribute these discrepancies to uncertainties in the calculation, e.g., still not perfectly converging results with cell size.

Considering all observations and arguments together, we have converging evidence supporting the attribution of the axial (hh and kk) pairs to PLX1/PLX2 (0.998–0.999 eV) double peak, and the basal hk and kh configurations to PLX3 (1.014 eV) and PLX4 (1.051 eV), respectively. Following this assignment, the energy order of the PL associated to the different configurations appears identical to the one currently accepted for the divacancy $(V_C V_{Si})^0$ ZPLs [23], and displayed as PL1–PL4 in Fig. 4. This analogy is in agreement with very similar EPR signatures resulting from nearly identical magnetization densities, as previously established in Ref. [27] and illustrated again in Figs. 4(a) and 4(c). This analogy is also found in the charge transfer associated with the ZPL emission as shown in Fig. 5. In a one-particle picture the $^3E \rightarrow {}^3A_2$ transition of the axial pairs is related to an

TABLE I. Comparison between experimental ZPL energies for the divacancies and the NV^- pair (axial hh/kk and basal hk/kh orientations) in 4H-SiC with transition energies calculated within DFT using the HSE06 hybrid functional. Former experimental data for the divacancies from Ref. [23] are also given.

	Divacancy $(V_C V_{Si})^0$			NV pair $(N_C V_{Si})^-$	
Defect orientation	DFT (eV)	Expt. (eV) (ZPL)	Expt. [23] (eV)	DFT (eV)	Expt. (eV) (ZPL)
kk	1.05	1.095 (PL1)	1.09	0.97	0.998 (PLX1)
hh	1.06	1.095 (PL2)	1.10	0.99	0.999 (PLX2)
hk	1.08	1.119 (PL3)	1.12	1.00	1.014 (PLX3)
kh	1.10	1.150 (PL4)	1.15	1.02	1.051 (PLX4)

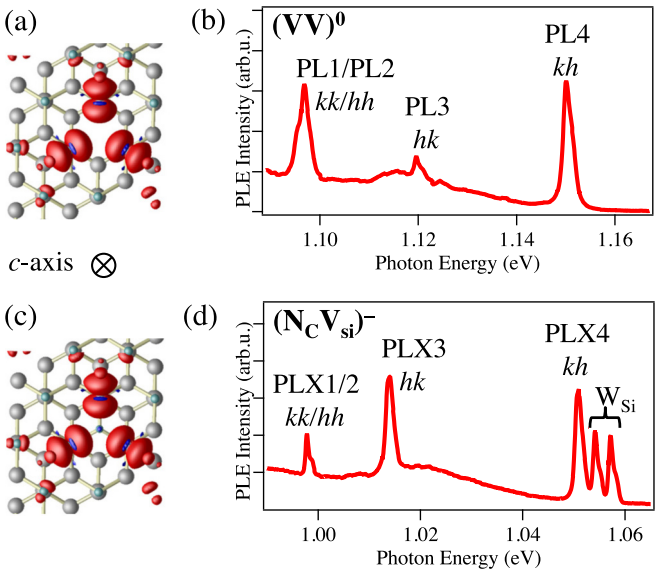

FIG. 4. ZPL assignment to axial and basal configurations of $(N_C V_{Si})^-$ and analogy with the divacancy $(V_C V_{Si})^0$. (a),(c) DFT-calculated magnetization densities for the axial (*hh*) divacancy and NV^- center, respectively (view along the hexagonal *c* axis) [27], showing strong similarity. (b) Divacancy PL1–PL4 association to the different configurations, as already established [23] (1.409 eV excitation). (d) Zoom on Fig. 2(b) PL spectra (PLX1–PLX4 lines) excited at 1.240 eV and tentatively associated to $(N_C V_{Si})^-$ configurations (based on the DFT-calculated transition energies; see Table I).

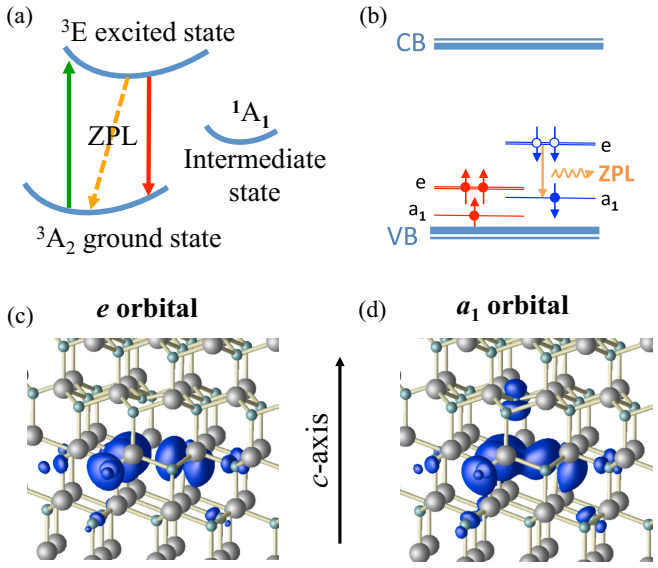

FIG. 5. Charge transfer associated with the ${}^3E \rightarrow {}^3A_2$ transition of the axial $N_C V_{Si}$ pairs (C_{3v} symmetry). (a) Optical excitation (green arrow), PL (red), and ZPL (dashed, orange arrow) processes. (b) One-particle schematics: from the *e*-like highest energy occupied molecular orbital of the ${}^3E$ excited state a spin-down electron goes back into the a_1-like hole (ground state configuration), giving rise to the ZPL emission. VB/CB: valence/conduction band. (c), (d) Spatial distribution of the *e*-like and a_1-like orbitals for the axial (*hh*) pair.

internal transition within the spin-down channel, whereby an electron from the *e*-like level falls back into the a_1-like level. Figures 5(c) and 5(d) show the DFT calculated density distributions of the corresponding orbitals. Besides the small *p*-like contribution to the a_1 orbital at the N_C site, the charge transfer is predominantly reflected in symmetry: whereas the a_1-like orbital provides a nearly rotationally symmetric distribution, the excited *e* orbital consists of three dangling bonds, well separated by three nodal planes. For both sets of pairs, $N_C V_{Si}$ centers as well as $V_C V_{Si}$ divacancies, the ZPL energies of the basal configurations are calculated to be slightly higher than the axial ones. This can be rationalized by the lower C_{1h} symmetry of the basal pairs. As a consequence, in the case of the axial pairs each of the twofold degenerate *e* orbitals [see Fig. 5(b)] splits into nondegenerate a' and a'' levels, both slightly more distant from the a_1 level, but predominantly localized at one and two carbon dangling bonds, respectively. This splitting opens two different excitation channels separated by about 50 meV. However, we use a nonresonant excitation which is followed by nonradiative relaxation into the lower energy excited state (with occupied a'' level), eventually leading to a single ZPL observed in emission for each pair.

Finally, we compared the PLE intensities of divacancy and NV centers. Figure 3(c) shows the intensity of PL1–PL4 ZPLs for the divacancy. We observe that they follow the same trend with increasing energy as expected from a given defect, and that there exists an optimal excitation energy at 1.409 eV [corresponding PL spectrum shown in Fig. 4(a)]. Moreover, the PL signal is significantly reduced at 1.240 eV. In comparison, $(N_C V_{Si})^-$ center-attributed lines PLX1–PLX4 intensities continuously increase in the excitation wavelength range explored. Moreover, these PLE measurements indicate that at 1.240 eV excitation energy we selectively suppress the underlying divacancy PL. This finding provides crucial leverage for optical detection of the magnetic resonance of the $(N_C V_{Si})^-$ in SiC, which has been so far challenging due to the overlap of NV ZPLs with divacancy phonon sidebands.

To conclude, cryogenic PLE spectroscopy on intentionally nitrogen-doped and proton irradiated 4*H*-SiC samples revealed the presence of a series of six distinct ZPLs in the energy range between 0.99 and 1.06 eV, in addition to the known four ZPLs of the $(V_C V_{Si})^0$ divacancy (PL1–PL4). Based on the comparison between PLE data and DFT calculations we were able to attribute four of these ZPLs (PLX1–PLX4) to different site orientations of the $(N_C V_{Si})^-$ defect pair. Moreover, the largest $(N_C V_{Si})^-$ ZPL intensity was observed at the smallest excitation energy of the tunable laser. At this 1.24 eV energy the divacancy emission is almost suppressed and therefore does not contribute to nitrogen-vacancy PL background. These results constitute a crucial step towards the optical detection and manipulation of the ground state electron spin of the $(N_C V_{Si})^-$ center in 4*H*-SiC. The technologically mature SiC material should facilitate similar applications as those of NV^- in diamond.

We are grateful to M.-F. Barthe for sample irradiation, and to T. Barisien, C. Testelin, C. Gourdon, and L. Thevenard for stimulating discussions. J.-S.L. is a member of Institut Universitaire de France. This work was supported by two public

grants overseen by the French National Research Agency (ANR) as part of the "Investissement d'Avenir" program: one grant from the Laboratoire d'Excellence Physics Atoms Light (LabEx PALM, reference: ANR-10-LABX-0039-PALM) and the Ph.D. grant of S.A.Z. (reference: IDEX Paris-Saclay ANR-11-IDEX- 0003-02). The work was also funded by DFG (SPP-1601). The computational calculations have been done at the Paderborn Center for Parallel Computing (PC^2).

[1] D. D. Awschalom, L. C. Bassett, A. S. Dzurak, E. L. Hu, and J. R. Petta, Science **339**, 1174 (2013).

[2] M. W. Doherty, N. B. Manson, P. Delaney, F. Jelezko, J. Wrachtrup, and L. C. L. Hollenberg, Phys. Rep. **528**, 1 (2013).

[3] H. Bernien, B. Hensen, W. Pfaff, G. Koolstra, M. S. Blok, L. Robledo, T. H. Taminiau, M. Markham, D. J. Twitchen, L. Childress, and R. Hanson, ACS Nano **497**, 86 (2013).

[4] G. D. Fuchs, G. Burkard, P. V. Klimov, and D. D. Awschalom, Nat. Phys. **7**, 789 (2011).

[5] H. J. Mamin, M. Kim, M. H. Sherwood, C. T. Rettner, K. Ohno, D. D. Awschalom, and D. Rugar, Science **339**, 557 (2013).

[6] L. P. McGuinness, Y. Yan, A. Stacey, D. A. Simpson, L. T. Hall, D. Maclaurin, S. Prawer, P. Mulvaney, J. Wrachtrup, F. Caruso, R. E. Scholten, and L. C. L. Hollenberg, Nat. Nanotechnol. **6**, 358 (2011).

[7] F. Dolde, H. Fedder, M. W. Doherty, T. Nöbauer, F. Rempp, G. Balasubramanian, T. Wolf, F. Reinhard, L. C. L. Hollenberg, F. Jelezko, and J. Wrachtrup, Nat. Phys. **7**, 459 (2011).

[8] L. Rondin, J.-P. Tetienne, T. Hingant, J.-F. Roch, P. Maletinsky, and V. Jacques, Rep. Prog. Phys. **77**, 056503 (2014).

[9] P. Neumann, I. Jakobi, F. Dolde, C. Burk, R. Reuter, G. Waldherr, J. Honert, T. Wolf, A. Brunner, J. H. Shim, D. Suter, H. Sumiya, J. Isoya, and J. Wrachtrup, Nano Lett. **13**, 2738 (2013).

[10] R. Schirhagl, K. Chang, M. Loretz, and C. L. Degen, Annu. Rev. Phys. Chem. **65**, 83 (2014).

[11] P. G. Baranov, A. P. Bundakova, A. A. Soltamova, S. B. Orlinskii, I. V. Borovykh, R. Zondervan, R. Verberk, and J. Schmidt, Phys. Rev. B **83**, 125203 (2011).

[12] A. L. Falk, B. B. Buckley, G. Calusine, W. F. Koehl, V. V. Dobrovitski, A. Politi, C. A. Zorman, P. X. L. Feng, and D. D. Awschalom, Nat. Commun. **4**, 1819 (2013).

[13] T. Umeda, N. T. Son, J. Isoya, E. Janzén, T. Ohshima, N. Morishita, H. Itoh, A. Gali, and M. Bockstedte, Phys. Rev. Lett. **96**, 145501 (2006).

[14] J. W. Steeds, Phys. Rev. B **80**, 245202 (2009).

[15] S. Castelletto, B. C. Johnson, V. Ivády, N. Stavrias, T. Umeda, A. Gali, and T. Ohshima, Nat. Mater. **13**, 151 (2014).

[16] K. Szász, V. Ivády, I. A. Abrikosov, E. Janzén, M. Bockstedte, and A. Gali, Phys. Rev. B **91**, 121201 (2015).

[17] T. Wimbauer, B. K. Meyer, A. Hofstaetter, A. Scharmann, and H. Overhof, Phys. Rev. B **56**, 7384 (1997).

[18] N. Mizuochi, S. Yamasaki, H. Takizawa, N. Morishita, T. Ohshima, H. Itoh, and J. Isoya, Phys. Rev. B **68**, 165206 (2003).

[19] M. Widmann, S.-Y. Lee, T. Rendler, N. T. Son, H. Fedder, S. Paik, L.-P. Yang, N. Zhao, S. Yang, I. Booker, A. Denisenko, M. Jamali, S. A. Momenzadeh, I. Gerhardt, T. Ohshima, A. Gali, E. Janzén, and J. Wrachtrup, Nat. Mater. **14**, 164 (2015).

[20] D. Simin, F. Fuchs, H. Kraus, A. Sperlich, P. G. Baranov, G. V. Astakhov, and V. Dyakonov, Phys. Rev. Appl. **4**, 014009 (2015).

[21] S. G. Carter, Ö. O. Soykal, P. Dev, S. E. Economou, and E. R. Glaser, Phys. Rev. B **92**, 161202 (2015).

[22] N. T. Son, P. Carlsson, J. ul Hassan, E. Janzén, T. Umeda, J. Isoya, A. Gali, M. Bockstedte, N. Morishita, T. Ohshima, and H. Itoh, Phys. Rev. Lett. **96**, 055501 (2006).

[23] W. F. Koehl, B. B. Buckley, F. J. Heremans, G. Calusine, and D. D. Awschalom, Nature (London) **479**, 84 (2011).

[24] D. J. Christle, A. L. Falk, P. Andrich, P. V. Klimov, J. U. Hassan, N. T. Son, E. Janzén, T. Ohshima, and D. D. Awschalom, Nat. Mater. **14**, 160 (2015).

[25] U. Gerstmann, E. Rauls, T. Frauenheim, and H. Overhof, Phys. Rev. B **67**, 205202 (2003).

[26] J. R. Weber, W. F. Koehl, J. B. Varley, A. Janotti, B. B. Buckley, C. G. Van de Walle, and D. D. Awschalom, Proc. Natl. Acad. Sci. USA **107**, 8513 (2010).

[27] H. J. von Bardeleben, J. L. Cantin, E. Rauls, and U. Gerstmann, Phys. Rev. B **92**, 064104 (2015).

[28] M. Wagner, B. Magnusson, W. M. Chen, E. Janzén, E. Sörman, C. Hallin, and J. L. Lindström, Phys. Rev. B **62**, 16555 (2000).

[29] G. Calusine, A. Politi, and D. D. Awschalom, arXiv:1510.02202.

[30] See Supplemental Material at http://link.aps.org/supplemental/10.1103/PhysRevB.94.060102 in which Fig. S1 displays room-temperature PL spectra under laser excitation at either 405, 532, or 633 nm wavelength; and Fig. S2 shows the low temperature (10 K) PL spectra under 423 nm (2.93 eV) and 1000 nm (1.24 eV) laser excitations wavelengths.

[31] J. Schneider, H. D. Müller, K. Maier, W. Wilkening, F. Fuchs, A. Dörnen, S. Leibenzeder, and R. Stein, Appl. Phys. Lett. **56**, 1184 (1990).

[32] J. Schneider and K. Maier, Phys. B (Amsterdam, Neth.) **185**, 199 (1993).

[33] A. Gällström, B. Magnusson, F. C. Beyer, and A. Gali, Phys. B (Amsterdam, Neth.) **407**, 1462 (2012).

[34] P. Giannozzi *et al.*, J. Phys.: Condens. Matter **21**, 395502 (2009).

[35] J. P. Perdew, K. Burke, and M. Ernzerhof, Phys. Rev. Lett. **77**, 3865 (1996).

[36] J. Heyd and G. E. Scuseria, J. Chem. Phys. **121**, 1187 (2004).